Title

Cytoskeletal organization in microtentacles

Journal

Experimental Cell Research, 357(2)

ISSN

0014-4827

Authors

Killilea, Alison N

Csencsits, Roseann

Le, Emily Bao Ngoc Thien

et al.

Publication Date

2017-08-01

DOI

10.1016/j.yexcr.2017.05.024

Peer reviewed

HHS Public Access

Author manuscript

Exp Cell Res. Author manuscript; available in PMC 2018 August 15.

Published in final edited form as:

Exp Cell Res. 2017 August 15; 357(2): 291–298. doi:10.1016/j.yexcr.2017.05.024.

Cytoskeletal Organization in Microtentacles

Alison N. Killilea[a,1], **Roseann Csencsits**[a,2], **Emily Le**[a], **Anand M. Patel**[a], **Samuel J. Kenny**[b], **Ke Xu**[a,b], and **Kenneth H. Downing**[a,*]

[1]Molecular Biophysics and Integrated Biomaging Division, Lawrence Berkeley National Laboratory Berkeley, CA 94720 USA

[2]Department of Chemistry, University of California Berkeley, CA 94720 USA

Abstract

Microtentacles are thin, flexible cell protrusions that have recently been described and whose presence enhances efficient attachment of circulating cells. They are found on circulating tumor cells and can be induced on a wide range of breast cancer cell lines, where they are promoted by factors that either stabilize microtubules or destabilize the actin cytoskeleton. Evidence suggests that they are relevant to the metastatic spread of cancer, so understanding their structure and formation may lead to useful therapies. Microtentacles are formed by microtubules and contain vimentin intermediate filaments, but beyond this, there is little information about their ultrastructure. We have used electron microscopy of high pressure frozen sections and tomography of cryo-prepared intact cells, along with super resolution fluorescence microscopy, to provide the first ultrastructural insights into microtubule and intermediate filament arrangement within microtentacles. By scanning electron microscopy it was seen that microtentacles form within minutes of addition of drugs that stabilize microtubules and destabilize actin filaments. Mature microtentacles were found to be well below one micrometer in diameter, tapering gradually to below 100 nanometers at the distal ends. They also contained frequent branches and bulges suggestive of heterogeneous internal structure. Super resolution fluorescence microscopy and examination of sectioned samples showed that the microtubules and intermediate filaments can occupy different areas within the microtentacles, rather than interacting intimately as had been expected. Cryo-electron tomography of thin regions of microtentacles revealed densely packed microtubules and absence of intermediate filaments. The number of microtubules ranged from several dozen in some areas to just a few in the thinnest regions, with none of the regular arrangement found in axonemes. Improved understanding of the mechanism of microtentacle formation, as well as the resultant structure, will be valuable in developing therapies against metastasis, if the hypothesized role of microtentacles in metastasis is confirmed. This work provides a significant step in this direction.

[*]Corresponding author. Kenneth H. Downing, Donner Laboratory, Lawrence Berkeley National Laboratory, Berkeley, CA 94720 USA, Tel 510-486-5941; fax 510-486-6488.

[1]present address: Department of Molecular and Cell Biology, University of California, Berkeley, CA 94720 USA

[2]present address: Schafer Vallecitos Laboratories, Inc. Sunol, CA 94586 USA

Keywords

microtentacles; structure; electron tomography; microtubules; metastasis

Introduction

Upon escape from the extracellular matrix, mammary epithelial cells extend long microtubule-based protrusions termed microtentacles (McTNs), dynamic structures that can promote cell attachment [1, 2]. A number of factors that promote the appearance of McTNs are found to be elevated in cancers, particularly in advanced stages. The correlation of these enhanced McTN-producing factors with cancer progression, along with the ability of McTNs to increase reattachment of circulating tumor cells, implicates McTNs in metastasis. McTNs were originally identified by the presence of a form of tubulin in which the C-terminal tyrosine of α-tubulin has been removed, leaving a glutamic acid at the end of the peptide chain [1]. Tubulin is commonly cycled between these two states, termed Glu-tubulin and Tyr-tubulin, by activity of an as-yet uncharacterized peptidase and a tubulin tyrosine ligase (TTL) [3], respectively. Glu-tubulin is commonly associated with more stable microtubules (MTs) *in vivo*, although there appears to be little difference in the stability of MTs formed *in vitro* with either type of tubulin [4]. Rather, the difference may relate to preferential association of other factors with one or the other type of tubulin. In particular, vimentin intermediate filaments appear to associate more strongly with Glu-tubulin and contribute to MT stability [5, 6]. Immediately following cell detachment, Glu-tubulin increases ~40 fold as a result of decreased TTL activity [1]. Vimentin, whose upregulation is a common marker of metastatic cancer progression and a predictor of poor prognosis, colocalizes with tubulin in McTNs, as seen by immunofluorescence microscopy [7]. Functionally, its overexpression leads to more stable McTNs, as there is a strong correlation between the level of vimentin expression in various breast cancer cell lines and the presence of McTNs on the cells [7]. It can thus be reasonably predicted that vimentin plays a role in stabilizing the MTs and thus the McTNs, and that the MT and IF networks would be closely associated. In the absence of elevated vimentin expression, other MT-stabilizing factors, including tau overexpression and the presence of Taxol, have been found to promote McTNs [1, 7–10].

Microtentacles are distinct from cilia and flagella, the only other commonly known thin, dynamic microtubule-based projections. A few other microtubule-based projections have been observed, including aberrant cilia seen on breast cancer cells [11], “tubulopodia” on T-cells [12], and neurite outgrowths driven by MT sliding [13]. Whether McTNs bear any relation to these in composition or structure remains to be seen as structural information about each emerges. McTNs are clearly quite distinct from more commonly encountered cell extensions such as filopodia, cytonemes, lamellapodia and invadopodia, which are all actin-based. While actin depolymerization results in retraction of these other structures, it promotes extension and stabilization of McTNs [1].

This effect appears to be a reflection of the counterbalancing forces and complementary activities of the microtubule and actin components of the cytoskeleton [2]. Disruption of the

normal balance is seen in a number of ways in cancer. For example, circulating tumor cells (CTCs) have an altered cytoskeleton that is protective against the deformation caused by shear stress in the vasculature and also allows them to deform and squeeze through the narrow capillaries. These effects are frequently associated with a decrease in the activity of actin crosslinking factors that normally stiffen the cell [14, 15]. It has been found that the ratio of F-actin to G-actin decreases as malignancy proceeds, reflecting the loss of a stable actin network [16]. These changes correlate with an increased propensity for McTN formation.

While McTNs are distinct from invadopodia in their response to actin depolymerization, they do share much of the same machinery. Both structures have MTs, IFs composed of vimentin, kinesin, and actin filaments, but the relative amounts of each appear to be greatly different in the two structures. In McTNs tubulin is the major protein and the amount of actin may be vanishingly small, while invadopodia are generally seen to be primarily formed of actin with at most only few MTs.

The MTs in McTNs are substantially more stable than the majority of MTs within the cell body. While MTs in cells normally turn over within minutes, in McTNs they may have a lifetime over 12 hours [1]. Association with IFs may be just one of several stabilizing factors, and it has become clear that any of the factors that stabilize MTs, such as vimentin, tau or MT-stabilizing drugs, correlate with stabilization of McTNs. Increasing MT stability enhances the activity of McTNs in cell reattachment [8]. The stabilizing factor with perhaps the most clinical relevance is Taxol, which functions as an anti-cancer agent by stabilizing MTs. Taxol has also been shown to stabilize McTNs and lead to more active attachment, while microtubule depolymerizing agents such as colchicine reduce attachment [17]. A critical question with clinical implications is whether Taxol treatment, which is highly effective against many types of primary tumors, actually promotes the metastasis and relapse to a drug-resistant cancer that is frequent among breast cancer patients.

Characterization by fluorescence light microscopy has provided much of what is currently known about McTN structure and activity. Studies have been carried out on a number of breast cancer cell lines as well as samples from cancer patients [1, 7–10]. So far there has been no suggestion of structural differences in McTNs among the different cell lines or of any dependence of their structure on the presence of MT-stabilizing drugs or actin-destabilizing drugs. A fundamental understanding of McTN structure and characterization of its response to drugs such as Taxol should help to understand the physical and mechanical basis of these responses. Here we have used a variety of imaging techniques to provide the first ultrastructural data revealing the arrangement of MTs and IFs inside of McTNs.

Materials and Methods

Cells and Reagents

The MDA-MB-231 cell line used in this work was a generous gift from the Bissell lab. Cells were cultured in RPMI GlutaMax (Life Technologies Inc.) supplemented with 10% fetal bovine serum (Hyclone) and 1% PenStrep at 37 °C with 5% CO_2. To prevent cell-substratum adhesion and promote the suspended state after detachment with trypsin, cells were

resuspended in serum-free media with DMSO as vehicle control or serum free media with a final concentration of 5μM latrunculin A and 1.7μM Taxol (paclitaxel) on ultralow attachment plates (Corning). Cells were routinely cultured until 60–70% confluent before detachment, exposure to drug and preparation for visualization. All chemicals and reagents were purchased from Sigma-Aldrich, unless otherwise noted.

Scanning Electron Microscopy

A timed series of control and drug-treated cells were transferred from ultra-low attachment plates to silicon nitride wafers coated with 0.1 % polylysine and then fixed with 2.5% glutaraldehyde in 0.1M cacodylate buffer at pH 7.2. After dehydration in a graded series of ethanol the samples were critical point dried and sputter coated with gold-palladium. Samples were viewed on a JEOL-6010plus SEM.

Immunocytochemistry

After exposure to drugs on low-attachment plates, cells were transferred to glass coverslips coated with 0.1% polylysine. They were fixed with a solution of 3% paraformaldehyde and 0.1% glutaraldehyde in PBS, followed by two rinses with 0.1% sodium borohydride in PBS. Cells were permeabilized and blocked using a solution of 0.5% Triton X-100 and 3% BSA in PBS. Coverslips were co-incubated with 1 μg/ml monoclonal mouse anti-α-tubulin antibody (Clone DM1A; Sigma T9026) and 5 μg/ml monoclonal rabbit anti-human vimentin (Abcam ab92547) in blocking buffer overnight at 4 °C. Cells were washed three times with 0.2% BSA and 0.1% Triton X-100 in PBS followed by incubation with 5 μg/ml goat-anti-mouse IgG1 secondary antibody conjugated with Alexa Fluor 647 (Invitrogen A21240) and 5 μg/ml donkey-anti-rabbit secondary antibody (Jackson ImmunoResearch 711-005-152) labeled with CF680 (Biotium 92139) for 1 hr at room temperature. Cells were then rinsed three times with washing buffer.

STORM imaging

Dye-labeled cell samples were mounted on glass slides with a standard STORM imaging buffer consisting of 5% (w/v) glucose, 200 mM cysteamine, 0.8 mg/ml glucose oxidase, and 40 μg/ml catalase in 1M Tris-HCL (pH 7.5) [18, 19]. Coverslips were sealed using Cytoseal 60. STORM imaging was performed on a homebuilt setup based on a modified Nikon Eclipse Ti-U inverted fluorescence microscope using a Nikon CFI Plan Apo λ 100× oil immersion objective (NA 1.45). Dye molecules were photoswitched to the dark state and imaged using a 647-nm laser (MPB Communications); a 405-nm laser was used concurrently to reactivate fluorophores into the emitting state. 647- and 405-nm lasers were passed through an acousto-optic tunable filter and introduced through an optical fiber into the back focal plane of the microscope and onto the sample at intensities of ~2 kW cm^{-2} and ~1 W cm^{-2}, respectively. The power of the 405-nm laser (typical range 0–1 W cm^{-2}) was adjusted during image acquisition so that at any given instant, only a small, optically resolvable fraction of the fluorophores in the sample were in the emitting state. A translation stage was used to shift the laser beams towards the edge of the objective so that light reached the sample at incident angles slightly smaller than the critical angle of the glass-water interface. Emission of Alexa Fluor 647 and CF680 was collected concurrently and split into two light paths using a dichroic mirror (T685lpxr; Chroma). Each light path was projected

onto one half of an Andor iXon Ultra 897 EM-CCD camera. Data were collected at a framerate of 110 Hz for a total of ~80,000 frames per image. Image reconstruction was performed according to previously described methods [18, 19]. A ratiometric detection scheme [20, 21] was employed for two-color STORM imaging. Dye assignment was performed by first localizing and recording the intensity of switching events in each image path. Localizations in both image paths corresponding to the same activated molecule were identified based on matching their super-localized positions and assigned a color based on their intensity ratios between the two paths [20, 21].

High Pressure-Frozen Resin Embedded Sections

Suspended MDA-MB-231 cells were applied to sapphire discs coated with 0.1 % polylysine and fixed with 2% paraformaldehyde and 0.5% glutaraldehyde in 0.1M cacodylate buffer pH 7.2. Discs were then high pressure frozen using a Leica EMPACT2-RTS high pressure freezer (Leica Microsystems). Super-Quick Freeze Substitution (SQFS) was performed in 1% osmium tetroxide and 0.1% uranyl acetate (UA) in acetone as previously described [22]. LR White resin was used for infiltration, and polymerized blocks were post-fixed and stained with 1% osmium tetroxide and 0.5% UA. 70nm thick sections were cut on a Reichert-Jung Ultracut E ultramicrotome, placed on formvar-coated 200 mesh hexagonal grids and post-stained in UA and lead citrate. Sections were viewed on a Philips CM200 electron microscope at 200 kV and images were collected on a Gatan Ultrascan CCD camera.

Cryo Electron Tomography

Cells were deposited onto 200 mesh lacey grids that had been glow discharged and coated with 10 nm colloidal gold, blotted with Whatman #1 filter paper for 6 seconds and plunged into liquid ethane for cryo preservation using a manual cryo plunge apparatus [23]. Tilt series were recorded on a JEOL-3100-FEF electron microscope at 2 degree intervals between ~−60/+60 with a pixel size of 0.44 nm on the specimen and defocus of ~5 μm. Low dose methods were used with SerialEM [24] controlling data acquisition. Images were collected on a 4k decelerator-CCD [25]. Image alignment was done using the gold fiducials with IMOD [26]. The final tomograms were computed using the SIRT algorithm in Tomo3d [27]. Display and segmentation of volumes were done with IMOD.

Results

Scanning Electron Microscopy (SEM)

SEM imaging provides substantially higher resolution than the conventional light microscopy that has been previously used in studying McTNs. We have used SEM to visualize McTNs at the early stages of their formation following exposure to cytoskeleton-altering drugs. We treated suspended MDA-MB-231 breast cancer cells with Taxol and latrunculin (LA) to induce formation of McTNs. Samples were prepared for SEM at various times to track the development of McTNs after drug treatment. As seen in Fig. 1, within one minute of adding LA and Taxol, the cells have produced numerous surface blebs, presumably as an effect of the collapsing actin cytoskeleton. By 3 minutes, McTNs have begun to form, and at 5 minutes they are well developed and often up to ten micrometers

long. Figure 2 shows an isolated cell after 60 min treatment which has a characteristic distribution of McTNs. These have diameters well below 1 μm, some thinner than 100 nm even near the cell body, and lengths of tens of micrometers. They taper slowly to smaller diameters along their length. There are also frequent branches along the McTNs, as well as structures that appear as “bubbles” or membranous blebs. These features were not evident in earlier light micrographs.

Superresolution Fluorescence imaging

Using 3D stochastic optical reconstruction microscopy (3D-STORM) we imaged MTs and vimentin IFs in latrunculin- and Taxol-treated suspended MDA-MB-231 breast cancer cells with ~20 nm resolution. At this resolution, these two components of the cytoskeleton are well resolved from each other. Figure 3 shows a cell with a prominent McTN about 8 μm long. A bundle of MTs that originates in the cell body extends out into the McTN. Vimentin extends into this protrusion as well. Within the cell body there is limited overlap between vimentin and tubulin, and it appears that some degree of this separation of the two components continues out into the McTN. As has been seen in previous work [1], there are regions of the McTN that are predominantly rich in either tubulin or vimentin, suggesting that the two networks may be more spatially separated than might have been expected based on the notion that vimentin directly stabilizes MTs within the McTNs. There are areas of high tubulin content that are virtually devoid of vimentin, and vice versa. Furthermore, even in areas of the McTN that appear to show a close association between MTs and IFs in the xy-plane (Fig. 3b), a virtual cross-section reveals that the two targets may be spatially distinct (Fig. 3c). Thus, the high resolution and 3D capability of STORM imaging allow us to get a sense of the scale of this separation.

Mapping MT and IF Networks Using High Pressure-Frozen Resin Embedded Sections

To examine regions of McTNs that are too thick to penetrate with the electron beam (typically more than 500 nm thick), drug-treated cells were high-pressure frozen, embedded in resin and sectioned for conventional TEM. Figure 4 shows a region of a McTN in which both MTs and IFs are well resolved. In regions such as this that are fairly close to the cell body, the MTs generally appear to cluster into small groups, while the IFs appear more widely dispersed. The separation of MTs and IFs is readily apparent in this image and is generally comparable to what is seen by STORM within the cell body. In these proximal regions the cytoplasm appears as an extension of the normal cell interior, with numerous ribosomes and occasional mitochondria, although no ER is evident. Farther out in the McTN there are regions where the two networks are closely apposed, but in most of the image they are well separated to the point of appearing independent. It thus seems that the MTs and IFs retain their rather independent localizations for some distance into the McTNs.

Figure 5 shows a larger region of a McTN as it emerges from the cell body and tapers to a size where just a few MTs are visible in the section. We have traced the MTs and IFs visible in this section to show how distant the two networks tend to be (Fig. 5b). Close associations between them are rare, and the number of IFs falls off faster than the MTs on moving into the farther distal region.

Cryo Tomography

In regions of the McTN that are sufficiently thin, on the order of a few hundred nanometers, it is possible to obtain high quality tomographic data from unstained, frozen-hydrated samples in order to provide a highly detailed description of the molecular arrangement within the McTN. These specimens were prepared by simply applying cells to an EM grid and plunge freezing with no stain or fixation and are thus expected to provide the best depiction of the actual structure. Figure 6a shows a low magnification view of a cell in one of these preparations. The cell body is too thick for appreciable penetration by the beam, but close inspection shows many thin projections from the cell into regions where the ice is thin enough for high resolution imaging. We have recorded tomograms of these areas in which bundles of MTs are seen with resolution sufficient to resolve the protofilament structure of the MTs. However, we do not see IFs in these very thin regions, although they would be expected to be about twice the size of tubulin protofilaments. We have on occasion seen IFs in adjacent areas, indicating that resolving them is not a problem, but they do not appear in close association with the MTs.

Figure 6b is a section through one 3-D tomographic reconstruction of a McTN that is about 150 nm thick. Cross sections through this tomogram, such as shown in Fig. 6c, show from 9 to 13 MTs, decreasing toward the distal end. Figure 6d is a model of the MTs within this area. The MTs are quite densely packed, but are not organized in any apparent way as they would be, for example, in an axoneme. There are occasional ends of MTs in regions where the diameter of the McTN is decreasing, and some of these have distinctive capping structures. We presume that these are plus ends, given that most MTs originate with their minus ends near the MT organizing center (MTOC) within the cell body. While we have also seen apparent minus-ends of MTs, they generally appear near complementary plus ends in regions that show distortions suggesting damage, and we conclude that these ends arise from breakage of the MTs during preparation. It is evident that almost all of the ends visible are related to the decreasing diameter of the McTN as they become thinner away from the cell body. The general lack of minus ends suggests that all of the MTs originate within the cell, likely at the MTOC, and polymerize at the distal end of the McTN as it extends. Figure 7 shows electron tomograms of several other McTNs that contain from just a few MTs to several dozen. These represent the extremes of what we have imaged by cryo-tomography and the range of MT arrangements within the McTNs.

Discussion

The fact that approximately 90% of all cancer deaths are caused by metastatic spread from the primary tumor [28] highlights a need to understand the interaction of CTCs with their environment as they explore and search for favorable sites for reattachment, as well as the mechanisms involved in reattachment. The demonstration that McTNs enhance reattachment of cells *in vitro* and *in vivo* suggests that they play an important role in metastasis, and the strong correlation between cancer progression and factors that promote both McTN formation and cell attachment supports this hypothesis [7–10, 17, 29–32]. Factors that promote McTN formation, particularly actin depolymerization, give the CTCs a strong survival advantage in the circulation. Many of the factors that stabilize McTNs, such as high

vimentin or tau expression and decreased tubulin tyrosine ligase activity, are known to be substantially enhanced as cancer develops and are frequently associated with more advanced or aggressive cancers. Many of these factors are characteristics of the epithelial-to-mesenchymal transition that is associated with cancer progression [10].

Taxol is a particularly interesting factor in this context, as its administration is associated only with detectable cancer and thus at a stage where numerous CTCs may be present. There are indications that Taxol has a substantial effect on CTCs even before reattachment. In one study, the number of CTCs increased by a factor of 1000 – 10,000 following treatment with epirubicin and cyclophosphamid followed by Taxol compared to those receiving just the epirubicin/cyclophosphamid [33], suggesting that Taxol may either help cells escape from the primary tumor or promote survival within the circulation. The combination of increased lifetime of CTCs and higher probability of reattachment poses a potential danger to long-term patient survival which could be brought about by treatment with taxanes and other MT-stabilizing drugs, or by actin-destabilizing drugs. Better characterization of the structural components of the McTN should improve our understanding of how drugs could be used to target them and of the functional and structural basis of their responses.

In this work we have focused on the MDA-MB-231 breast cancer cell line. Under some conditions these cells, as well as other breast cancer cell lines and CTCs taken from patients, spontaneously produce McTNs [1, 7]. In these experiments we have enhanced the expression of McTNs by exposure of the cells to Taxol and latrunculin. We find that McTNs develop rapidly, within minutes following drug administration to cells that have been detached for 15 minutes. The distribution of tubulin and vimentin in these McTNs appears similar by fluorescence light microscopy to what has been seen before [1], with general overlap between regions where the two proteins are plentiful but occasional regions where one dominates over the other. A high degree of overlap would be expected based on the observations of enhanced Glu-tubulin in McTNs and preferential association of vimentin with Glu-tubulin that results in stabilized MTs. From the STORM images it is clear that the concentrations of both tubulin and vimentin are much greater in the McTNs than in the cell body. The TEM images of sections support this observation, with a greater concentration of both MTs and IFs within the McTNs than in the cell body. At the resolution of our STORM images, though, it becomes clear that the two proteins are not as tightly associated as expected. A 3D examination of our STORM images shows that while MTs and IFs may appear to overlap in the xy-plane, they may in fact be spatially distinct when viewed in three dimensions. This is even more evident when the McTNs are examined by electron microscopy where both MTs and IFs are easily resolved. Particularly in thicker parts of the McTNs, near the cell body, the MT and IF networks are still quite sparse and there is little indication of interactions between them. Proceeding out from the cell body the density of both MTs and IFs increases with their increasing confinement in the narrowing McTN, but there is no apparently greater association between them. Toward the distal regions of the McTNs, as they become thin enough that we can obtain higher resolution images by cryo-tomography, we find that the MTs dominate, even to the exclusion of IFs. These regions are thin enough that they are more difficult to capture in thin sections, but the sections of very thin regions that we have studied have a similar dearth of IFs, even though they would be visible with more contrast than in the unstained cryo samples. On the other hand, the MTs

are densely packed. As shown in Fig. 7, we have found McTNs in proximal regions where there are upwards of 30 MTs and no apparent other components, as well as regions many micrometers long with just a few MTs.

All of the MTs observed within the McTNs are conventional singlet MTs, as opposed to the doublets of flagella, and where we have reached sufficient resolution to count the number of protofilaments, they all have 13, as in most cellular MTs. We find frequent MT ends that we interpret as the plus-end termini of MTs that extend from within the cell body. The lack of points of initiation of new MTs within the McTNs suggests that the MTs are oriented with the plus ends distal to the cell, as is the case in flagella and consistent with the usual MT orientation.

McTNs form within extensions of the cell membrane, driven by polymerization of the MTs. In cilia and flagella the mechanical forces involved in this extension arise from simultaneous polymerization of the 9 doublet MTs, in which there is generally an extension of the A-tubule beyond the B-tubule within the complete doublet. These 9 MTs are further supported by the dyneins and other proteins that link them into a relatively rigid structure. Clearly, though, the strength of this structure is not required for membrane extension. The typical 9+2 arrangement of MTs within flagella appears to have evolved from arrangements that had as few as 3 MTs and are still present in some primitive organisms [34]. Thus only a few MTs are sufficient to generate enough force to produce membrane-bound extensions. Microtubule-driven extensions of liposome membranes have also been observed [35], although in that work it was not possible to determine the number of MTs involved. Calculations suggested that a single MT would be sufficient. Tubulin is actively transported to the site of polymerization in growing axonemes and flagella, but it seems unlikely that the intraflagellar transport system that carries tubulin to the growing end would be involved in McTN growth, particularly in the absence of MT doublets. Thus it is an interesting question how McTN polymerization occurs so rapidly at such substantial distances out from the cell body. Less is known about the polymerization of IFs, but the same question arises in the case of vimentin, presuming that its polymerization also occurs near the growing end rather than in or near the cell body, which would require transport of the assembled IF network along the McTN.

The lack of clear interaction between MTs and IFs is one of the major surprises in this work. The strong correlation between the level of vimentin overexpression and the production of McTNs on various cell lines suggested that the vimentin and MT network interact strongly to stabilize the MTs and thus promote the presence of McTNs. Our data show that these filaments are not always contiguous, and that when they are present in the same region of a McTN they may be separated by as much as 200 nm. It is plausible that a protein such as plectin or kinesin could link these two networks, even over such a large distance. Plectin is known to interact with both tubulin and vimentin and to crosslink MTs and IFs within neurons [36], and in its extended form may be 200 nm in length. Within the narrower McTNs, of course, the MTs and IFs are constrained to be much closer than this. Plectin and vimentin have also recently been shown to be the most highly overexpressed proteins in a strongly metastatic prostate cell line [37], suggesting that the presence of plectin could

contribute to McTN stability. There is also evidence that kinesin is involved in regulating the interactions of vimentin and tubulin in a mechanism that is more active with Glu-tubulin [5].

It is possible that the conditions of rapid growth induced by drug treatment in these studies does not produce the same balance of components as may be present in CTCs. For example, although we allow time between detachment and drug treatment for conversion of Tyr-tubulin to Glu-tubulin and we see substantial amounts of vimentin within the MTs, it may be that longer times are required for a physiologically relevant interaction to develop between them. The conversion of tubulin reaches a steady state within an hour alter detachment [1], so on the time scale of our experiments we expect that there would be substantial amounts of Glu-tubulin; it remains to be seen how dependent McTN formation is upon the Taxol and/or latrunculin concentration.

Conclusions

We have examined the structure of McTNs that form on detached cells in the presence of Taxol and latrunculin. By light microscopy, these drug-induced McTNs are indistinguishable from those that arise spontaneously following detachment. In the case of detachment-induced McTN formation, the conversion of Tyr-tubulin to Glu-tubulin appears to favor a MT-stabilizing action of vimentin IFs, resulting in extension of the McTNs. It is apparent that an altered actin cytoskeleton is also important for the appearance of McTNs, and the different levels of actin crosslinking and bundling factors in the various cell lines are one factor in determining their propensity to express McTNs. The addition of both Taxol and latrunculin enhances both MT stability and depletion of the actin network, producing substantial numbers of McTNs on most cells. The concentrations of tubulin and vimentin are greatly increased within the McTNs over those in the rest of the cell, reflecting the observation of higher densities of MTs and IFs seen by electron microscopy. We find little evidence of a direct interaction between the MTs and IFs, which may reflect MT stabilization by Taxol rather than vimentin. The organization of MTs, particularly in thin regions of the McTNs where they can be studied by cryo-EM and tomography, shows them to be quite densely packed with no obvious bridging structures such as seen in axonemes.

Acknowledgments

This research is supported by National Institutes of Health Grant No. GM051487 to KHD and NSF grant CHE-1554717 and the Pew Biomedical Scholars Award to KX. We are grateful to Kent McDonald for help with preparing high-pressure frozen samples for electron microscopy.

List of abbreviations

CTC	circulating tumor cell
IF	intermediate filament
LA	latrunculin
McTN	microtentacle
MT	microtubule

SEM	scanning electron microscope
STORM	stochastic optical reconstruction microscopy
TEM	transmission electron microscope
UA	uranyl acetate

References

1. Whipple RA, Cheung AM, Martin SS. Detyrosinated microtubule protrusions in suspended mammary epithelial cells promote reattachment. Exp Cell Res. 2007; 313:1326–1336. [PubMed: 17359970]
2. Matrone MA, Whipple RA, Balzer EM, Martin SS. Microtentacles tip the balance of cytoskeletal forces in circulating tumor cells. Cancer Res. 2010; 70:7737–7741. [PubMed: 20924109]
3. Ersfeld K, Wehland J, Plessmann U, Dodemont H, Gerke V, Weber K. Characterization of the tubulin-tyrosine ligase. J Cell Biol. 1993; 120:725–732. [PubMed: 8093886]
4. Kumar N, Flavin M. Modulation of some parameters of assembly of microtubules in vitro by tyrosinolation of tubulin. Eur J Biochem. 1982; 128:215–222. [PubMed: 7173203]
5. Kreitzer G, Liao G, Gundersen GG. Detyrosination of tubulin regulates the interaction of intermediate filaments with microtubules in vivo via a kinesin-dependent mechanism. Mol Biol Cell. 1999; 10:1105–1118. [PubMed: 10198060]
6. Skoufias DA, Wilson L. Assembly and colchicine binding characteristics of tubulin with maximally tyrosinated and detyrosinated alpha-tubulins. Arch Biochem Biophys. 1998; 351:115–122. [PubMed: 9500839]
7. Whipple RA, Balzer EM, Cho EH, Matrone MA, Yoon JR, Martin SS. Vimentin filaments support extension of tubulin-based microtentacles in detached breast tumor cells. Cancer Res. 2008; 68:5678–5688. [PubMed: 18632620]
8. Charpentier M, Martin S. Interplay of Stem Cell Characteristics, EMT, and Microtentacles in Circulating Breast Tumor Cells. Cancers. 2013; 5:1545–1565. [PubMed: 24240660]
9. Matrone MA, Whipple RA, Thompson K, Cho EH, Vitolo MI, Balzer EM, et al. Metastatic breast tumors express increased tau, which promotes microtentacle formation and the reattachment of detached breast tumor cells. Oncogene. 2010; 29:3217–3227. [PubMed: 20228842]
10. Whipple RA, Matrone MA, Cho EH, Balzer EM, Vitolo MI, Yoon JR, et al. Epithelial-to-mesenchymal transition promotes tubulin detyrosination and microtentacles that enhance endothelial engagement. Cancer Res. 2010; 70:8127–8137. [PubMed: 20924103]
11. Reilova-Velez J, Seiler MW. Abnormal cilia in a breast carcinoma. An ultrastructural study. Arch Pathol Lab Med. 1984; 108:795–797. [PubMed: 6089697]
12. Arkhipov SN, Maly IV. Microtubule appendages mediating T-cell motility and polarity. Integr Biol (Camb). 2015; 7:1143–1153. [PubMed: 25797390]
13. del Castillo U, Lu W, Winding M, Lakonishok M, Gelfand VI. Pavarotti/MKLP1 regulates microtubule sliding and neurite outgrowth in Drosophila neurons. Curr Biol. 2015; 25:200–205. [PubMed: 25557664]
14. Cha HJ, Jeong MJ, Kleinman HK. Role of thymosin beta4 in tumor metastasis and angiogenesis. J Natl Cancer Inst. 2003; 95:1674–1680. [PubMed: 14625258]
15. Magdalena C, Dominguez F, Loidi L, Puente JL. Tumour prothymosin alpha content, a potential prognostic marker for primary breast cancer. Br J Cancer. 2000; 82:584–590. [PubMed: 10682670]
16. Katsantonis J, Tosca A, Koukouritaki SB, Theodoropoulos PA, Gravanis A, Stournaras C. Differences in the G/total actin ratio and microfilament stability between normal and malignant human keratinocytes. Cell Biochem Funct. 1994; 12:267–274. [PubMed: 7834816]
17. Balzer EM, Whipple RA, Cho EH, Matrone MA, Martin SS. Antimitotic chemotherapeutics promote adhesive responses in detached and circulating tumor cells. Breast Cancer Res Treat. 2010; 121:65–78. [PubMed: 19593636]

18. Rust MJ, Bates M, Zhuang X. Sub-diffraction-limit imaging by stochastic optical reconstruction microscopy (STORM). Nat Methods. 2006; 3:793–795. [PubMed: 16896339]
19. Huang B, Wang W, Bates M, Zhuang X. Three-dimensional super-resolution imaging by stochastic optical reconstruction microscopy. Science. 2008; 319:810–813. [PubMed: 18174397]
20. Bossi M, Folling J, Belov VN, Boyarskiy VP, Medda R, Egner A, et al. Multicolor far-field fluorescence nanoscopy through isolated detection of distinct molecular species. Nano Lett. 2008; 8:2463–2468. [PubMed: 18642961]
21. Testa I, Wurm CA, Medda R, Rothermel E, von Middendorf C, Folling J, et al. Multicolor fluorescence nanoscopy in fixed and living cells by exciting conventional fluorophores with a single wavelength. Biophys J. 2010; 99:2686–2694. [PubMed: 20959110]
22. McDonald KL, Webb RI. Freeze substitution in 3 hours or less. J Microsc. 2011; 243:227–233. [PubMed: 21827481]
23. Comolli LR, Duarte R, Baum D, Luef B, Downing KH, Larson DM, et al. A portable cryo-plunger for on-site intact cryogenic microscopy sample preparation in natural environments. Microsc Res Techniq. 2012; 75:829–836.
24. Mastronarde DN. Automated electron microscope tomography using robust prediction of specimen movements. J Struct Biol. 2005; 152:36–51. [PubMed: 16182563]
25. Downing KH, Mooney PE. A charge coupled device camera with electron decelerator for intermediate voltage electron microscopy. Rev Sci Instrum. 2008; 79:043702. [PubMed: 18447528]
26. Kremer JR, Mastronarde DN, McIntosh JR. Computer visualization of three-dimensional image data using IMOD. J Struct Biol. 1996; 116:71–76. [PubMed: 8742726]
27. Agulleiro JI, Fernandez JJ. Fast tomographic reconstruction on multicore computers. Bioinformatics. 2011; 27:582–583. [PubMed: 21172911]
28. Chaffer CL, Weinberg RA. A perspective on cancer cell metastasis. Science. 2011; 331:1559–1564. [PubMed: 21436443]
29. Balzer EM, Whipple RA, Thompson K, Boggs AE, Slovic J, Cho EH, et al. c-Src differentially regulates the functions of microtentacles and invadopodia. Oncogene. 2010; 29:6402–6408. [PubMed: 20956943]
30. Bhandary L, Whipple RA, Vitolo MI, Charpentier MS, Boggs AE, Chakrabarti KR, et al. ROCK inhibition promotes microtentacles that enhance reattachment of breast cancer cells. Oncotarget. 2014; 6:6251–6266.
31. Perry NA, Vitolo MI, Martin SS, Kontrogianni-Konstantopoulos A. Loss of the obscurin-RhoGEF downregulates RhoA signaling and increases microtentacle formation and attachment of breast epithelial cells. Oncotarget. 2014; 5:8558–8568. [PubMed: 25261370]
32. Vitolo MI, Boggs AE, Whipple RA, Yoon JR, Thompson K, Matrone MA, et al. Loss of PTEN induces microtentacles through PI3K-independent activation of cofilin. Oncogene. 2013; 32:2200–2210. [PubMed: 22689060]
33. Camara O, Rengsberger M, Egbe A, Koch A, Gajda M, Hammer U, et al. The relevance of circulating epithelial tumor cells (CETC) for therapy monitoring during neoadjuvant (primary systemic) chemotherapy in breast cancer. Ann Oncol. 2007; 18:1484–1492. [PubMed: 17761704]
34. Prensier G, Vivier E, Goldstein S, Schrevel J. Motile flagellum with a "3 + 0" ultrastructure. Science. 1980; 207:1493–1494. [PubMed: 7189065]
35. Elbaum M, Fygenson DK, Libchaber A. Buckling microtubules in vesicles. Phys Rev Lett. 1996; 76:4078–4081. [PubMed: 10061186]
36. Svitkina TM, Verkhovsky AB, Borisy GG. Plectin sidearms mediate interaction of intermediate filaments with microtubules and other components of the cytoskeleton. J Cell Biol. 1996; 135:991–1007. [PubMed: 8922382]
37. Burch TC, Watson MT, Nyalwidhe JO. Variable metastatic potentials correlate with differential plectin and vimentin expression in syngeneic androgen independent prostate cancer cells. PLoS One. 2013; 8:e65005. [PubMed: 23717685]

Highlights

- Microtentacles can form within minutes of the addition of inducing drugs and rapidly reach tens of micrometers in length with diameters in the range of a tenth of a micrometer
- Microtubules are clearly resolved in microtentacles by cryo-electron tomography
- There is little interaction between microtubules and intermediate filaments in drug-induced microtentacles

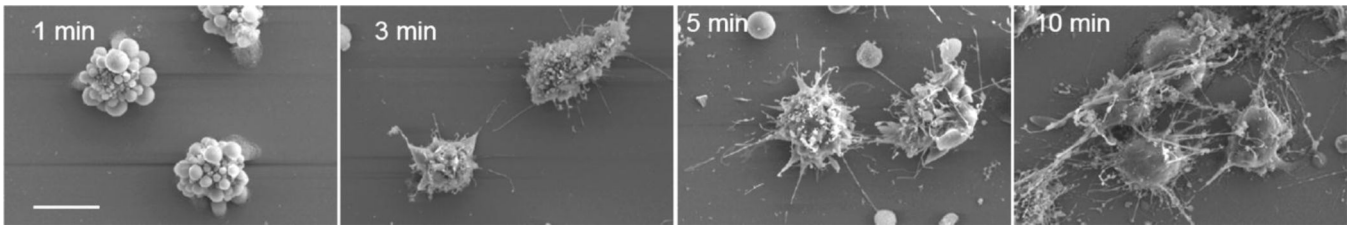

Figure 1.

Time course of McTN induction visualized by SEM. MDA-MB-231 cells were suspended over ultralow attachment plates, treated with 5μM latrunculin A and 1.7 μM Taxol for 1–10 minutes, then transferred to silicon nitride wafers and fixed. At 1 min cells already show substantial response to the drugs, with numerous blebs forming. By 3 min McTNs are beginning to appear, often seeming to emerge from the blebs. At 5 min the McTNs are up to 10 μm long. They continue to grow in length and number, and by 10 min appear to be involved in aggregation of the cells. Scale bar = 10 μm.

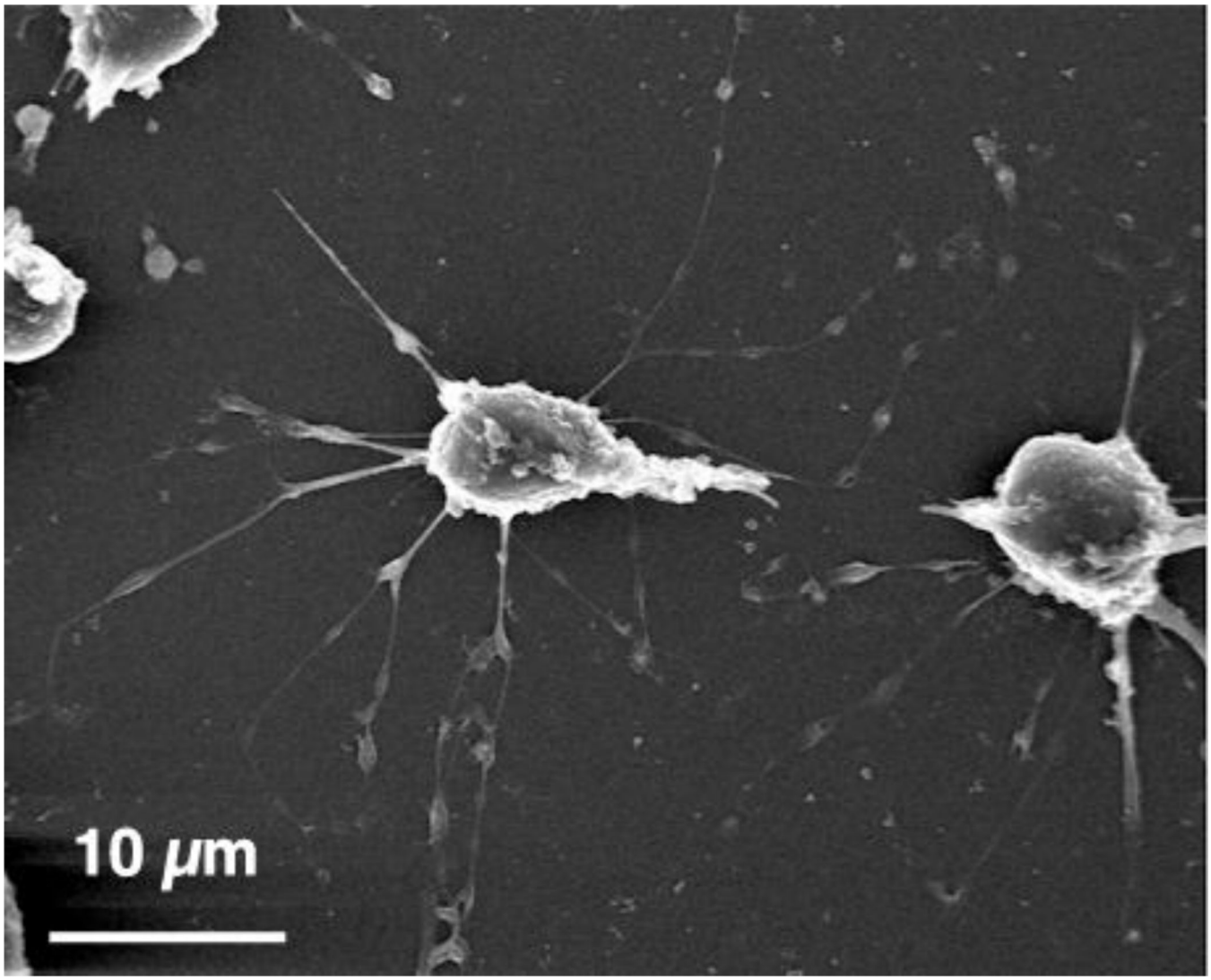

Figure 2.

SEM image of isolated cells after 60 min of exposure to latrunculin A and Taxol. Numerous McTNs are visible, all well below 1 μm in diameter and tens of μm long.

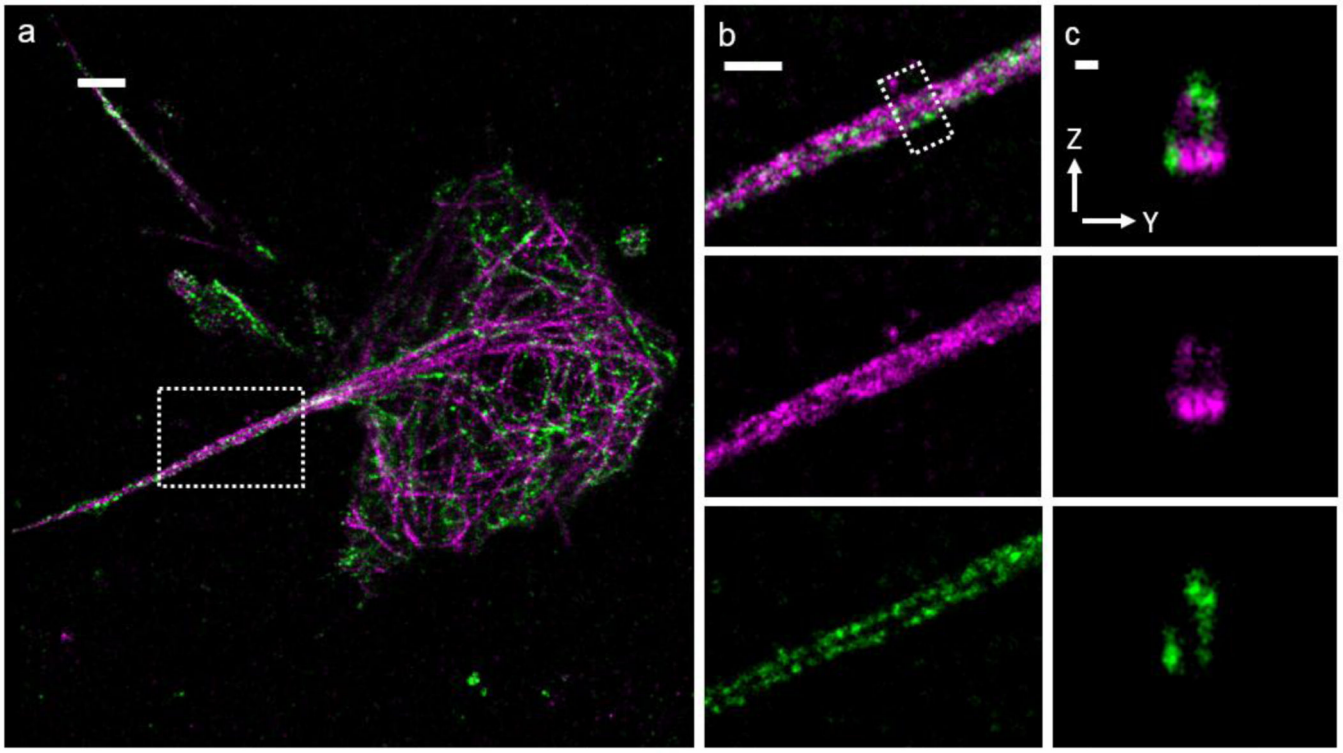

Figure 3.

A. STORM micrograph of an MDA-MB-231 cell that has been treated with LA and Taxol, then methanol-fixed and stained with antibodies for tubulin (magenta) and vimentin (green). The boxed area in the left image is shown enlarged (b), with the tubulin and vimentin channels separated. MTs can be seen originating in the cell body and extending into a prominent McTN along with vimentin. While there is substantial overlap in the two signals in the xy-plane, a virtual cross section (c) indicates that the MT and IF networks are not tightly coupled. Scale bars: 1 μm (a), 500 nm (b), 100 nm (c).

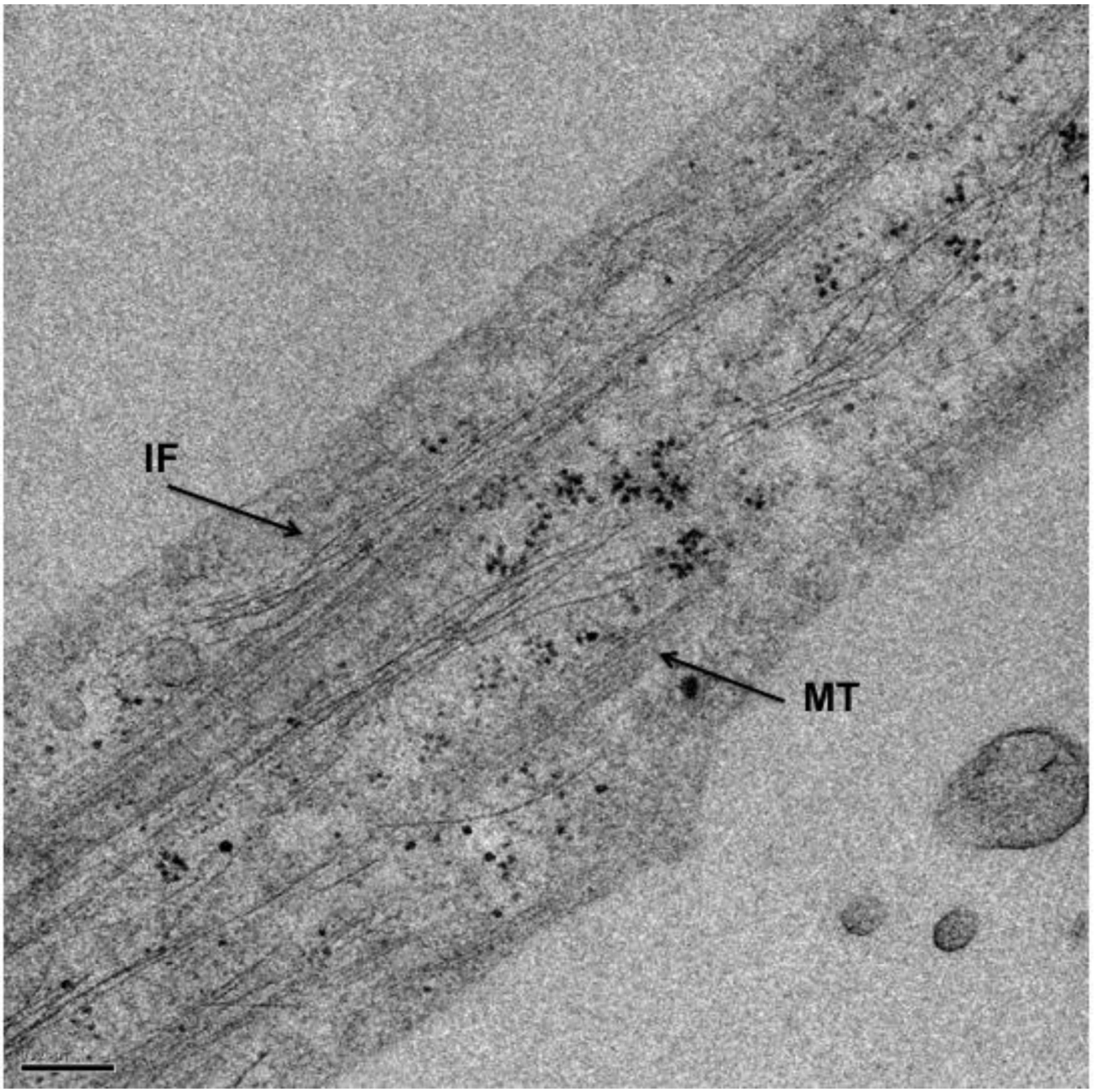

Figure 4.
TEM visualization of MTs and IFs within a McTN. In stained sections both of these cytoskeletal components are clearly visible. Other cellular components are also seen, particularly the darkly stained ribosomes. Scale bar = 100 nm.

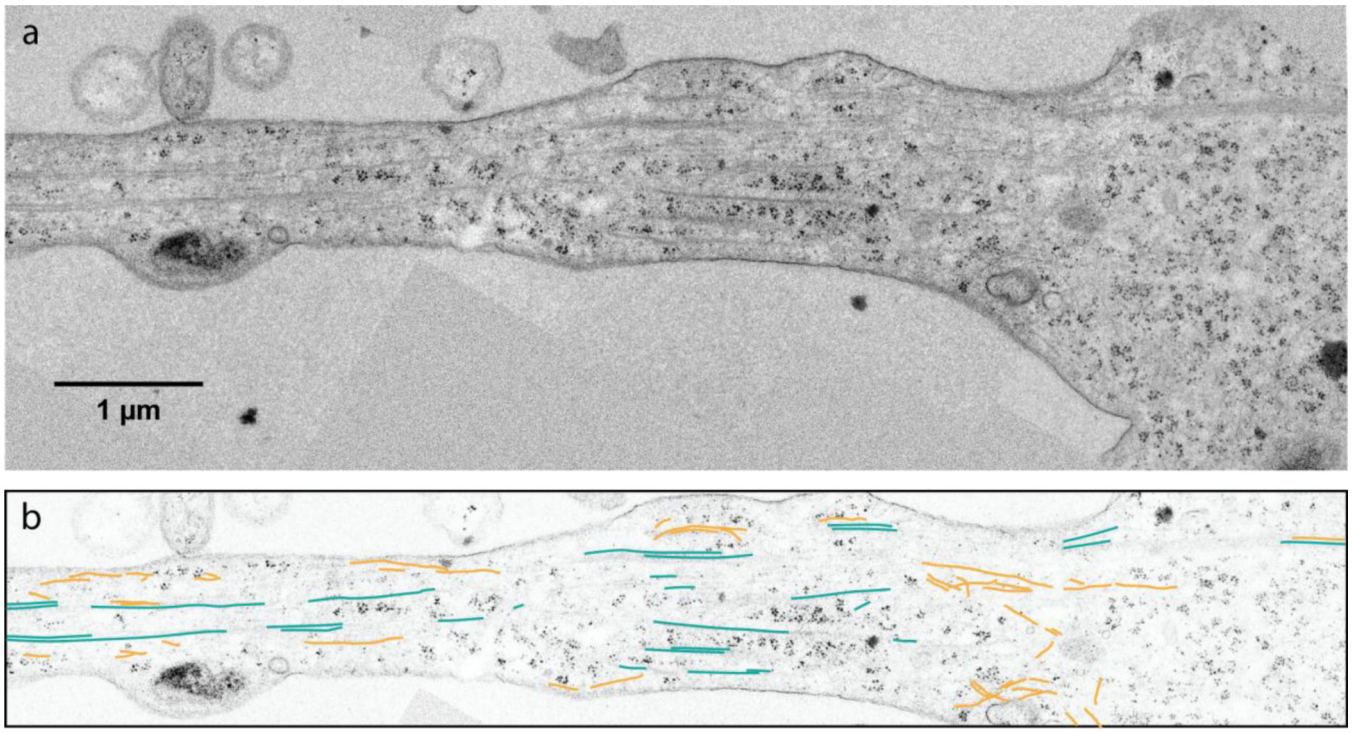

Figure 5.

TEM visualization of internal McTN structure in resin sections. The image (a) is a montage of micrographs of a McTN that was sectioned nearly parallel to its long axis. Microtubules and intermediate filaments are visible, although they are often found in different regions of the sample. In the schematic below (b) the most clearly resolved MTs and IFs are identified in blue and orange, respectively.

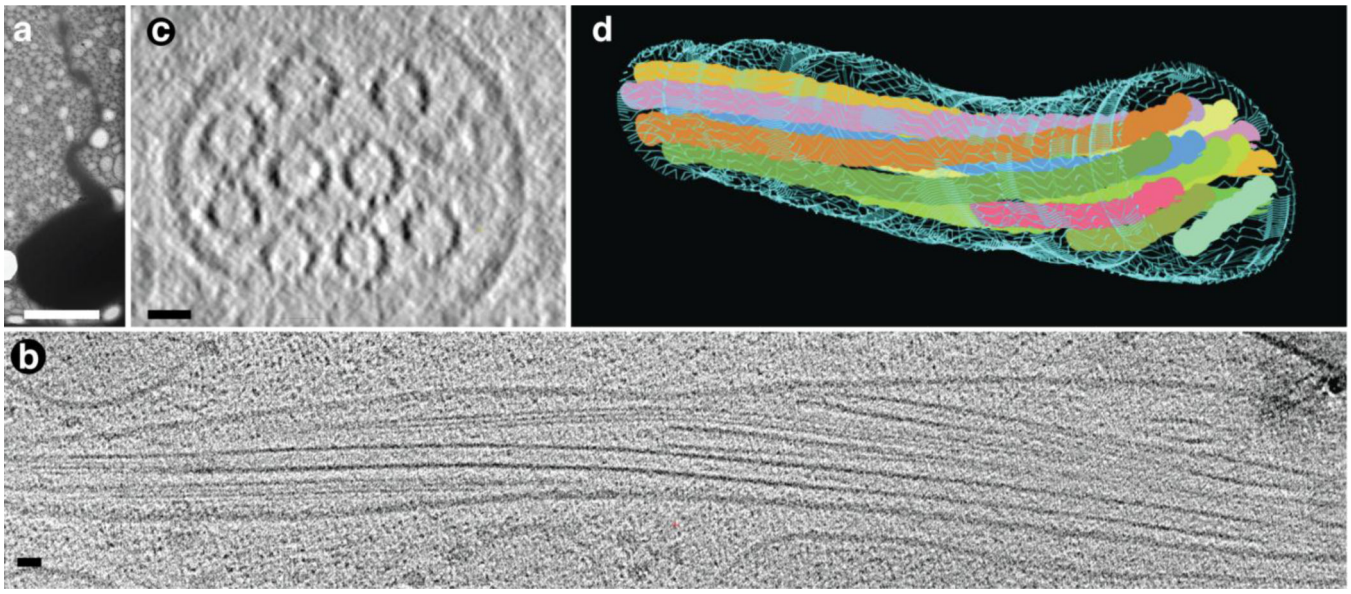

Figure 6.

Electron tomography of McTN. (a) Low magnification image of frozen-hydrated (unstained, unfixed) cell over lacy support film. One prominent McTN about 30 μm in length is visible, although the contrast is low due to the ice that embeds the specimen. Scale bar = 10 μm. (b) Section ~3 nm thick through 3D tomographic reconstruction obtained from a tilt series of low-dose images from another area. Parts of several microtubules can be seen passing up and down through this section. (c) Cross section through the reconstruction, showing that the MTs have 13 protofilaments and are quite closely packed in this region of the McTN. (d) Model for distribution of MTs enclosed by membrane of McTN, derived from full 3D map. Scale bars in (b) and (c) = 25 nm.

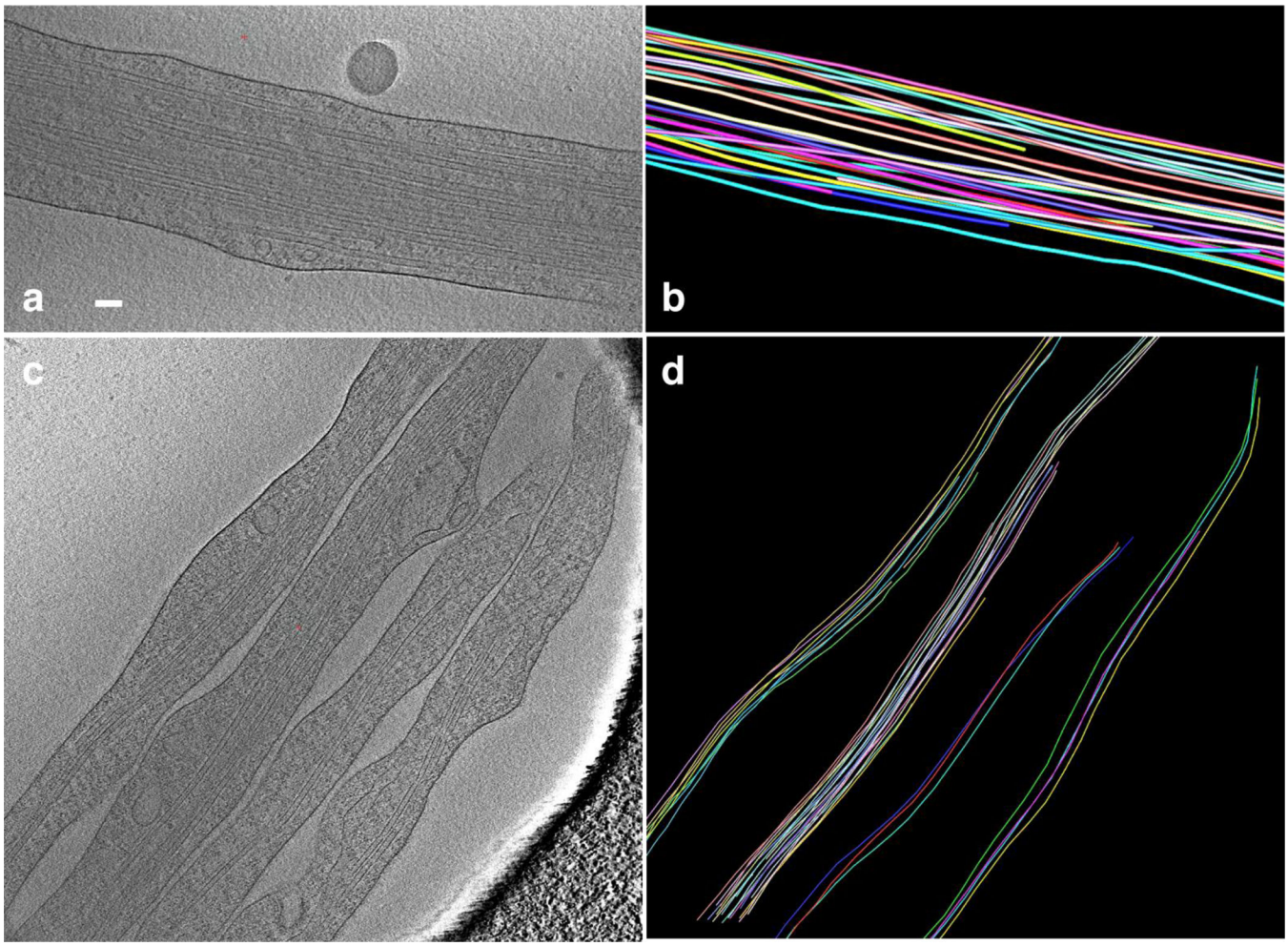

Figure 7.

The variety of MT distribution within McTNs, as seen by electron tomography. Top images (a, b) show a slice through a tomographic reconstruction of a relatively large McTN that contains over 20 MTs, which have been segmented for display in the model at the right. The bottom images (c, d) show a slice through the reconstruction of an area that contained four small McTNs with as few as 3 MTs and as many as 15, also displayed in the right image. Scale bar = 100 nm.